https://doi.org/10.3311/PPci.36589

Periodica Polytechnica Civil Engineering, 69(1), pp. 321–332, 2025

An Approximation of Yield Surface for Doubly Symmetrical Sections of Steel Structures

Hieu Nghia Hoang[1], Quoc Anh Vu[2*], Manh Hien Nghiem[2]

[1] Faculty of Construction Engineering, Haiphong University, 171 Phan Dang Luu, Kien An, 185100 Hai Phong, Vietnam
[2] Faculty of Civil Engineering, Hanoi Architectural University, Km 10, Nguyen Trai Street, Thanh Xuan District, 120500 Hanoi, Vietnam
[*] Corresponding author, e-mail: anhvq@hau.edu.vn

Received: 01 February 2024, Accepted: 26 November 2024, Published online: 05 December 2024

Abstract

The paper presents a new method to generate yield surfaces for the doubly symmetrical sections including thin-walled pipe, thin-walled box, and wide-flange I-shape under axial force combined with biaxial bending moments in nonlinear analysis of the steel frame. The yield surfaces are described by twenty parameters and all of them can be determined automatically by the computer program using the power and polynomial regressions of the interaction curves. The cutting plan algorithm (CPA) is adopted for internal force update to satisfy yield conditions in a plastic hinge. A computer code was designed to implement the proposed model and carry out nonlinear analyses on steel frames. Multiple computational examples have been executed to verify the proposed model's accuracy and efficiency, involving a comparison of results predicted by the proposed method with those obtained from alternative methods.

Keywords

yield surface, biaxial bending, doubly symmetrical sections, fiber model

1 Introduction

Nonlinear analysis is widely applied for steel frames in practical design. The most promising model for nonlinear analysis of the beam-column elements is the fiber method [1], where cross-sections of element are usually discretized into small fibers, and the nonlinear behavior of the material is represented by the uniaxial stress-strain relationship of a fiber. The fiber method is too computationally intensive for structures modelled by large number of elements [2, 3]. Therefore, it is usually applicable only for research purposes.

The fiber hinge method was introduced to overcome the above limitations of the fiber method [2–5]. Chiorean [6] introduced a novel formulation for determining the biaxial interaction diagrams and moment capacity contours of a composite steel-concrete cross-section. This approach employs an incremental, iterative procedure relying on arc-length constraint equations. However, the method, grounded in the fiber approach, may face challenges in determining the curvature of non-prismatic elements. This limitation can result in time-consuming structural analyses, as iterative solutions are typically employed in establishing yield surfaces.

The yield surface concept is required in the framework of the classical theory of plasticity and had been widely used in inelastic frame analysis to model the full plastification of the steel section under axial force combined with biaxial bending moment [7]. Deriving closed-form equations theoretically for the yield surface of a general section is complex. Therefore, the yield surfaces should be approximated by simple equations for practical nonlinear analyses of the structures. A smooth or single yield surface makes it relatively easy to satisfy the normality and yield criterion once plastic state reached [7].

The literature encompasses numerous methods proposed for conducting ultimate strength analyses on various sections, including wide-flange sections [8], as well as rectangular, circular, thin-walled pipe, thin-walled box, and wide-flange sections [7, 8]. These analyses are specifically focused on scenarios involving axial force combined with biaxial moments. Orbison et al. [7] proposed a polynomial expression for smooth yield surface that contained ratios of axial force and bending moments to the corresponding squash load and plastic moments. Orbison's equation was in excellent agreement with the plastification values except

Cite this article as: Hoang, H. N., Vu, Q. A., Nghiem, M. H. "An Approximation of Yield Surface for Doubly Symmetrical Sections of Steel Structures", Periodica Polytechnica Civil Engineering, 69(1), pp. 321–332, 2025. https://doi.org/10.3311/PPci.36589

significant errors occurred in the region of weak axis bending-axial force interaction in heavy I-shape sections. Duan and Chen [8] developed the yield surfaces that were smooth and convex in the three-dimension space that satisfied all special cases. For both the strong and weak axes of wide-flange I-shaped sections, the yield surfaces proposed by Duan and Chen [8] were below the theoretical yield surfaces.

Exact solutions for the yield surface of the wide-flange section were described by twelve equations depending on the location of the neutral axis [9] and nine equations proposed by Vu et al. [10] based on possible compression or tension areas caused by the axial force. The yield surface for wide-flange sections was also expressed by Morris and Fenves [11] using five equations. Other researchers [12–15] developed yield surfaces for steel I-sections and obtained results that matched very well to the theoretical yield surfaces. However, all those yield surfaces [10–15] were multiple-faceted surfaces. When multi-surface surfaces are used in the framework of the classical theory of plasticity, some difficulties may occur such as the derivatives of the yield function become indeterminate at the facet intersection [16], the elastic element forces must be checked against each facet, and forces at plastic hinges must be prevented from attempting to cross over from one facet to a neighboring facet [7], etc.

This paper proposes general yield surfaces of the doubly symmetrical sections of steel structures such as thin-walled pipe, thin-walled box, and wide-flange sections under axial force combined with biaxial bending moments. The developed equation for the yield surfaces result in:

1. an accuracy improvement of the yields surfaces to overcome the shortcoming of Duan and Chen equations [7] and Orbison equations [8];
2. single function in the three-dimension space that satisfied the requirement in the framework of the classical theory of plasticity;
3. reduction of the time-consuming process in comparison to the fiber model for the finite element analysis of the steel frame in the practical field.

Additionally, the cutting plan algorithm (CPA) is adopted for constraining the element forces on the yield surface in nonlinear analyses of the steel frames.

2 Yield surface

2.1 Section properties

Examine the cross-sections within the local coordinate system x-y-z, experiencing external bending moments around the y-axis and z-axis, along with an axial force along the x-axis, as illustrated in Fig. 1. Assumptions can be made for developing the yield surface of the cross sections as follows:

1. The plane section remains plane after deformation.
2. Shear and torsional interaction effects are not considered in the steel constitutive model.
3. The material is regarded as linear and elastic-perfectly plastic (strain hardening is ignored).
4. Local buckling and lateral torsional buckling are not involved.
5. Strains and deformations are small.
6. The roots at the intersection of flange and web are neglected.

The steel sections can be plastic and compact which can develop their full plastic moment without early interference by local buckling and lateral torsional buckling.

The axial yield strength and plastic moments can be expressed as follows:

$$\begin{aligned} P_y &= A_x f_y \\ M_{pz} &= Z_z f_y \\ M_{py} &= Z_y f_y \end{aligned} \tag{1}$$

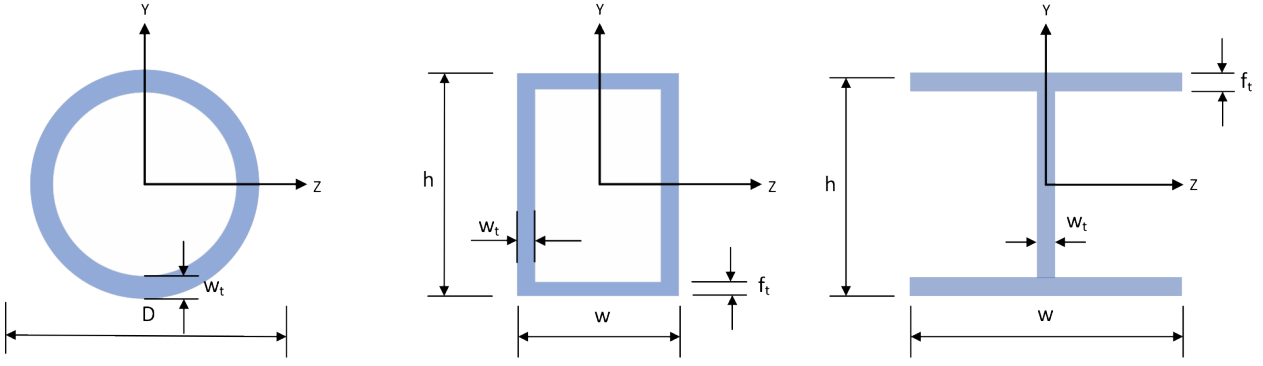

(a) (b) (c)

Fig. 1 Illustrations of doubly symmetrical sections: (a) Thin-walled pipe, (b) Thin-walled box, (c) Wide-flange I-shape

where f_y is strength of steel; P_y is axial yield strength; M_{pz} is plastic moment about z axis; M_{py} is plastic moment about y axis; and A_x is the cross-sectional area; and Z_z and Z_y are plastic moduli about z and y, respectively. The cross-sectional area and plastic moduli of thin-walled pipe, thin-walled box, and wide-flange I-shape are given in Table 1.

2.2 Proposed yield surface

The yield surface can be expressed in terms of the following non-dimensional quantities (Figs. 2 and 3):

$$p = \frac{|P|}{P_y};\ m_{pz} = \frac{|M_z|}{m_{pzp} M_{pz}};\ m_{py} = \frac{|M_y|}{m_{pyp} M_{py}} \tag{2}$$

where p is ratio of axial force to axial yield strength; P is axial load; P_y is axial yield strength; M_z is bending moment about z axis; M_y is bending moment about y axis; m_{pzp} and m_{pyp} are non-dimensional quantities as shown in Fig. 2 and calculated as:

$$\begin{aligned} m_{pzp} &= b_1 p^6 + b_2 p^4 + b_3 p^2 + 1 \\ m_{pyp} &= c_1 p^6 + c_2 p^4 + c_3 p^2 + 1 \end{aligned} \tag{3}$$

where b_1, b_2, b_3 are the polynomial regression coefficients of the p-m_{pzp} interaction curve; c_1, c_2, and c_3 are the polynomial regression coefficients of the p-m_{pyp} interaction curve. The fiber method can be utilized to generate interaction curves between axial forces and bending moments for a section, as shown in Fig. 2. The coefficients b_i and c_i are then determined using Eq. (3) through polynomial regression of the interaction curves.

The yield surface for a doubly symmetrical steel section as shown in Fig. 3 can be written in Eq. (4):

$$f = m_{pz}^{a_1} + m_{py}^{a_2} - 1 \tag{4}$$

where a_1 and a_2 are best fitting parameters dependent on sectional shapes. Equation (4) lacks apparent physical significance, but it can conform closely to a realistic physically derived yield surface [8].

3 Determination of parameters

3.1 Thin-walled pipe section

Since the plastic moments about z and y axes are the same at a certain axial load ratio then $a_1 = a_2 = 2$ for all thin-walled pipe sections. The exact solution of the yield surface for thin-walled pipe section proposed by Morris and Fenves [11] as:

$$m_{pzp} = \cos\left(\frac{\pi}{2} p\right). \tag{5}$$

Equation (5) can be expressed as Maclaurin series as follows:

$$m_{pzp} = 1 - \left(\frac{\pi}{2}\right)^2 \frac{p^2}{2!} + \left(\frac{\pi}{2}\right)^4 \frac{p^4}{4!} + \left(\frac{\pi}{2}\right)^6 \frac{p^6}{6!} + \ldots \tag{6}$$

or

$$m_{pzp} = 1 - 1.234 p^2 + 0.254 p^4 - 0.021 p^6 + \ldots. \tag{7}$$

The coefficients $b_1 = c_1 \approx -0.022$; $b_2 = c_2 \approx 0.257$; and $b_3 = c_3 \approx -1.235$, determined from polynomial regression

Table 1 Section properties

Sections	A_x	Z_z	Z_y
Thin-walled pipe	$\frac{\pi D^2}{4} - \frac{\pi (D-2w_t)^2}{4}$	$\frac{D^3}{12} - \frac{(D-2w_t)^3}{12}$	$\frac{D^3}{12} - \frac{(D-2w_t)^3}{12}$
Thin-walled box	$2hw_t + 2(w-2w_t)f_t$	$\frac{h^2 w_t}{2} + (w-2w_t) f_t (h-f_t)$	$\frac{w^2 f_t}{2} + (h-2f_t) w_t (h-w_t)$
Wide-flange I-shape	$hw_t + (w-w_t) f_t$	$\frac{h^2 w_t}{4} + (w-w_t) f_t (h-f_t)$	$\frac{w^2 f_t}{2} + (h-2f_t) \frac{w_t^2}{4}$

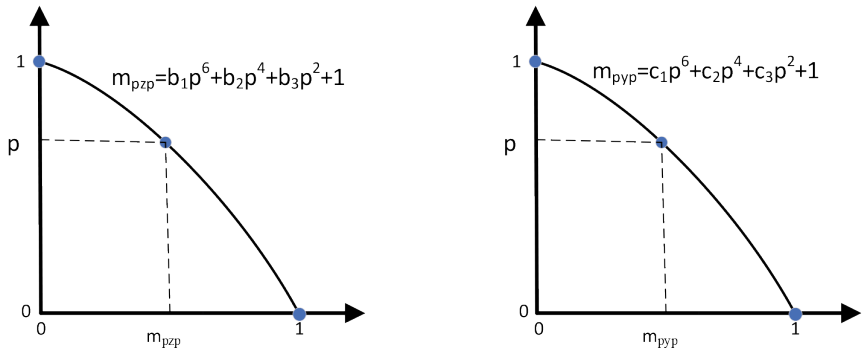

Fig. 2 Interaction curves between axial forces and bending moments

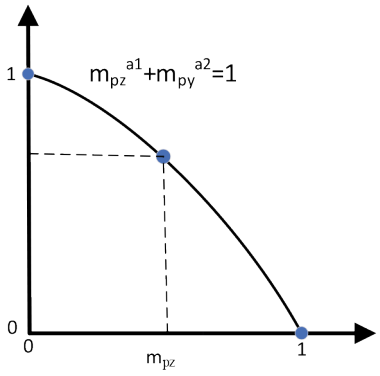

Fig. 3 Interaction curve between biaxial bending moments

in this study, are matched very well with the exact solution in Eq. (5).

3.2 Wide-flange and thin-walled box sections

The plastic moments change with bending axes from the *z*-axis to *y*-axis and the interaction curves of biaxial bending moments change their shape with the axial force ratios. As a result, a_1 and a_2 in Eq. (4) are not the same values and both are dependent on the axial force ratios. Equation (8) can be obtained by using the best fitting approach for a_1 and a_2:

$$\begin{aligned} a_1 &= d_1p^6 + d_2p^5 + d_3p^4 + d_4p^3 + d_5p^2 + d_6p + d_7 \\ a_2 &= e_1p^6 + e_2p^5 + e_3p^4 + e_4p^3 + e_5p^2 + e_6p + e_7 \end{aligned} \tag{8}$$

where d_1 to d_7, and e_1 to e_7 are coefficients of the polynomial regression. If the thin-walled box section is square and web and flange thicknesses are equal, then a_1 and a_2 are identical. The general shape of a_1 and a_2 are illustrated in Fig. 4. The fiber method can be utilized to generate interaction curves between biaxial bending moments for a section at different p values. Each curve provides a set of a_1 and a_2 using a best-fitting method. By applying Eq. (8) to these sets of a_1 and a_2 for polynomial regression, d_i and c_i coefficient can be determined.

4 Numerical solution

The element forces move tangent on the yield surface at plastic hinges when undergoing a transition from fully elastic state to fully plastic state. The plastic displacements may occur when a section of the column reaches a fully plastic state. The displacement increments can be separated into elastic and plastic components as follows:

$$d\boldsymbol{u} = d\boldsymbol{u}_e + d\boldsymbol{u}_p \tag{9}$$

where $d\boldsymbol{u}$ is total displacement increment; $d\boldsymbol{u}_e$ is elastic displacement increment; and $d\boldsymbol{u}_p$ is plastic displacement increment.

The elastic force increment can be expressed as:

$$d\boldsymbol{F} = \boldsymbol{K}\left(d\boldsymbol{u} - d\boldsymbol{u}_p\right) \tag{10}$$

where $\boldsymbol{K}$ is element stiffness matrix.

According to the flow rule, the plastic displacement increment is perpendicular to the potential surface and given by:

$$d\boldsymbol{u}_p = \lambda \frac{\partial \boldsymbol{g}}{\partial \boldsymbol{F}} = \lambda \boldsymbol{r} \tag{11}$$

where λ is plastic scalar or plastic parameter, which represents the magnitude of the plastic flow, $\lambda \geq 0$; g is potential function, for associate flow rule, $g = f$; $\boldsymbol{r}$ is flow direction, obtained upon differential of the plastic potential function with respect to forces.

Substituting Eq. (11) to Eq. (10) leads to:

$$d\boldsymbol{F} = \boldsymbol{K}\left(d\boldsymbol{u} - \lambda \boldsymbol{r}\right). \tag{12}$$

The force increments are related to the forces at the current time step and previous time step as:

$$d\boldsymbol{F} = \boldsymbol{F}_{n+1} - \boldsymbol{F}_n \tag{13}$$

where n is the time step.

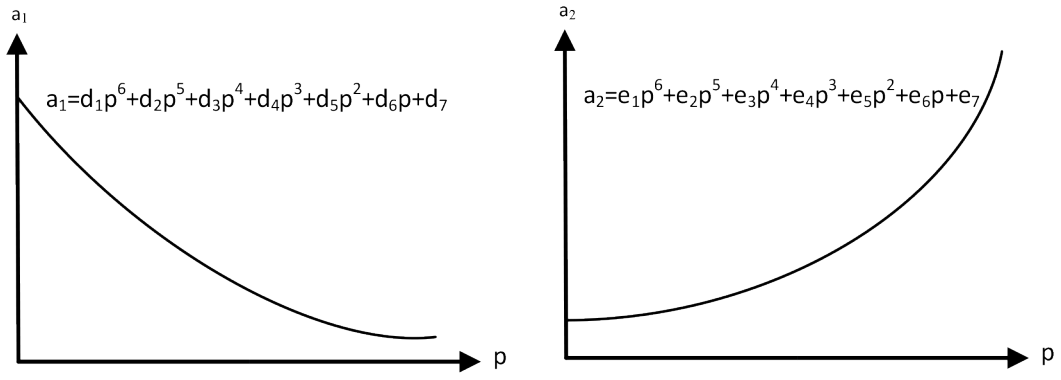

Fig. 4 The a_1 and a_2 functions for the wide-flange and thin-walled box sections

The forces at the current time step can be rewritten as:

$$\boldsymbol{F}_{n+1} = \boldsymbol{F}_n + \boldsymbol{K}d\boldsymbol{u} - \lambda \boldsymbol{K}\boldsymbol{r} \,. \tag{14}$$

The Backward Euler scheme [16] is carried out with total displacement increments to obtain an elastic predictor (point *B* in Fig. 5), by integrating the elastic equations. The first two terms of Eq. (14) represent elastic predictor as:

$$\boldsymbol{F}_{n+1}^{\text{trial}} = \boldsymbol{F}_n + \boldsymbol{K}d\boldsymbol{u} \,. \tag{15}$$

The elastically predicted forces are relaxed on a suitably updated yield surface (point *C* in Fig. 5) by correcting iteratively the plastic displacement increments along a direction specified by the plastic flow direction:

$$\boldsymbol{F}_{n+1} = \boldsymbol{F}_{n+1}^{\text{trial}} - \lambda \boldsymbol{K}\boldsymbol{r} \tag{16}$$

where $-\lambda \boldsymbol{K}\boldsymbol{r}$ is plastic corrector.

Consider force states as shown in Fig. 5, the force state at a point *C* on the yield surface is computed from the first order Taylor expansion of the yield function at point *B* as:

$$f_{(C)} = f_{(B)} + \boldsymbol{q}d\boldsymbol{F} \tag{17}$$

$$\boldsymbol{q} = \frac{\partial \boldsymbol{f}}{\partial \boldsymbol{F}} \tag{18}$$

where $\boldsymbol{q}$ is differential of the yield surface with respect to forces at point *B*.

By enforcing consistency of the yield function at point *C*:

$$f_{(B)} + \boldsymbol{q}\left(-\lambda \boldsymbol{K}\boldsymbol{r}\right) = 0 \,. \tag{19}$$

The plastic scalar can be obtained from Eq. (17) as:

$$\lambda = \frac{f_{(B)}}{\boldsymbol{q}\boldsymbol{K}\boldsymbol{r}} \,. \tag{20}$$

For the complicated yield surface such as the proposed yield surface in Eq. (4), the yield condition at point $C(f_{(C)})$ is usually not satisfied by the predicted forces in Eq. (16). The yield function $f_{(C)}$ is either greater or less than zero with significant error. The technique for constraining the element forces on the yield surface directly affects the accuracy and stability of the overall numerical solution. The implicit closest point projection method (CPPM) and the cutting plan algorithm (CPA) are two techniques (also known as return mapping technique) that were widely used in the literature [16–19], both were developed based on the backward Euler scheme [16]. The CPA itself avoids the need for second derivatives to be evaluated of the potential function making it easier to deal with complicated yield surfaces [18] so it was employed in this study. The complete force update using CPA algorithm is given in Appendix.

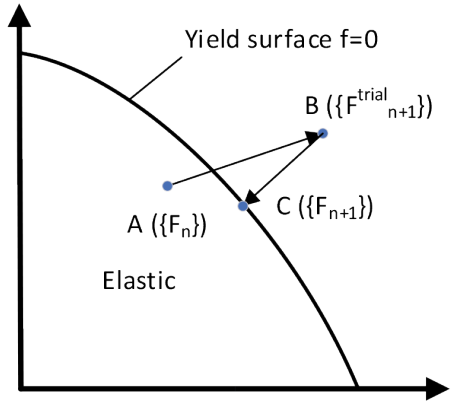

Fig. 5 Backward Euler scheme for associate plasticity

5 Numerical analyses and results

A computer program for **s**teel frame analysis using **p**lastic **h**inge approach (SPH) with fully graphical interface was developed based on the above algorithm for nonlinear analysis of three-dimensional steel frames. The analyses can be linear elastic, geometrically nonlinear, and materially and geometrically nonlinear. The program can generate the parameters for the yield surfaces of any thin-walled pipe, thin-walled box, and wide-flange I-shape cross sections using the proposed equations in this study.

5.1 Yield surfaces

Examples of the yield surfaces are performed for the thin-walled pipe, wide-flange, and thin-walled box sections to verify the proposed equations for p = 0.0, 0.3, 0.5, 0.7 and 0.9. The fiber method considered as the best approximation solution is used for the comparison purpose [2, 3].

For a thin-walled pipe section, the comparison of the yield surface contour is shown in Fig. 6. It can be observed that Eq. (4) with parameters presented in Table 2 and Table 3 can describe the behavior of a thin-walled section very well.

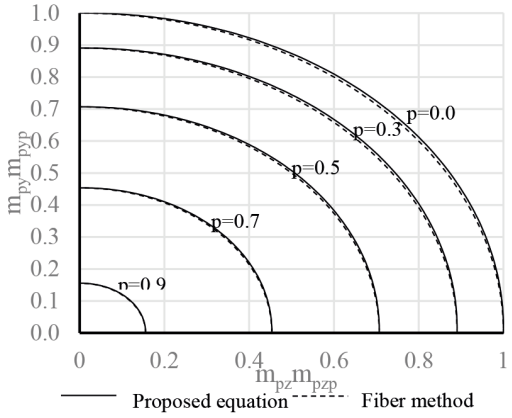

Fig. 6 Comparison of yield surfaces of thin-walled pipe section

Table 2 Parameters for p-m_{pzp} interaction curves

Parameters	Pipe	W12 × 30	HSS12 × 12 × 1/2
b_1	−0.022	−0.61	−0.083
b_2	0.257	1.48	0.537
b_3	−1.235	−1.87	−1.449
R^2	1.00	0.9998	0.9998

Table 3 Parameters for p-m_{pyp} interaction curves

Parameters	Pipe	W12 × 30	HSS12 × 12 × 1/2
c_1	−0.022	0.79	−0.083
c_2	0.257	−1.93	0.537
c_3	−1.235	0.15	−1.449
R^2	1.00	0.9998	0.9998

An accurate estimation for the yield surface of the thin-walled box HSS12 × 12 × 1/2 section is also obtained while comparing to the fiber method, as shown in Fig. 7 (a). Since plastic moments about z-axis and y-axis of are the same then the coefficients of the polynomial regression are also equal, $b_i = c_i$ (i = 1–3), $d_i = e_i$ (i = 1–7) in each axis as presented in Table 2 and Table 3.

Referring to yield surface contour for W12 × 30 section, the proposed equation, Orbison equation [7] and Duan and Chen equation [8] are plotted in Fig. 8 (a)–(c). It is observed that the interaction curves of the proposed model are in very good agreement with those of the fiber model except for the curve with p = 0.5 (in Fig. 8 (c)) where values of $m_{yp}m_{pyp}$ are slightly different from the plastification values. Conversely, the Orbison equation [7] and Duan and Chen equation [8] deviated from the fiber method. Fig. 8 (d) shows the variation of a_1 and a_2 which are approximated by the six-degree polynomials with parameters given in Table 4.

The accuracy of the proposed yield surfaces is evaluated by the coefficient of determination, R^2. For all sections, high accuracy of the proposed equation is obtained where all values of R^2 are greater than 0.99, as presented in Tables 2 to 4.

5.2 Steel columns

A three-dimensional, two-element column (Fig. 9) was analyzed to verify the proposed yield surfaces and the nonlinear solution algorithm. The element properties correspond to those of W6 × 20 and HSS6 × 6 × 1/4 sections of A36 steel. The applied loads were selected to ensure the maximum internal forces occur at the midspan node where the plastic hinge will be formed. Load increments were applied proportionally until constituting a collapse mechanism of the column with a plastic hinge formed at the midspan in each element. Values of F_x and F_y changed arbitrarily to obtain different plastic moments ratios.

Fig. 10 shows the interaction curves obtained from the fiber model for W6 × 20 and HSS6 × 6 × 1/4 sections, respectively. Fig. 10 also shows the internal force states of the elements at failure from the analyses. It can be observed that the internal force states at failure are very close to the plastification values. Table 5 presents the comparison of solution time between the fiber method and the proposed method. It can be observed that the solution time of the proposed method is 7.5 times to 84 times faster than that of the fiber method, dependent on the number of elements used in the analyses.

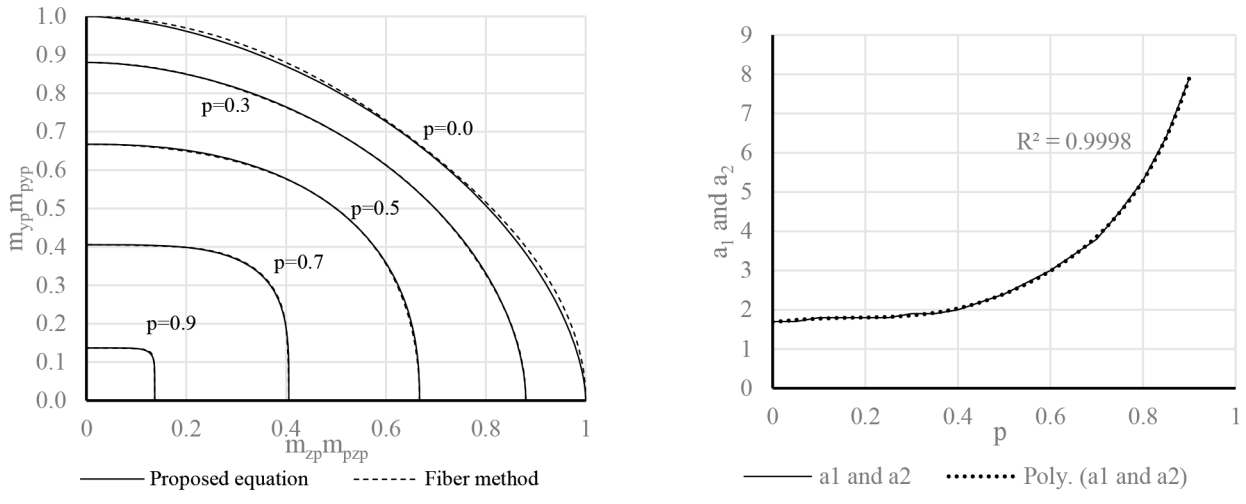

Fig. 7 Yield surface for HSS12 × 12 × 1/2 section: (a) Plan view of the yield surface, (b) a_1 and a_2 parameters

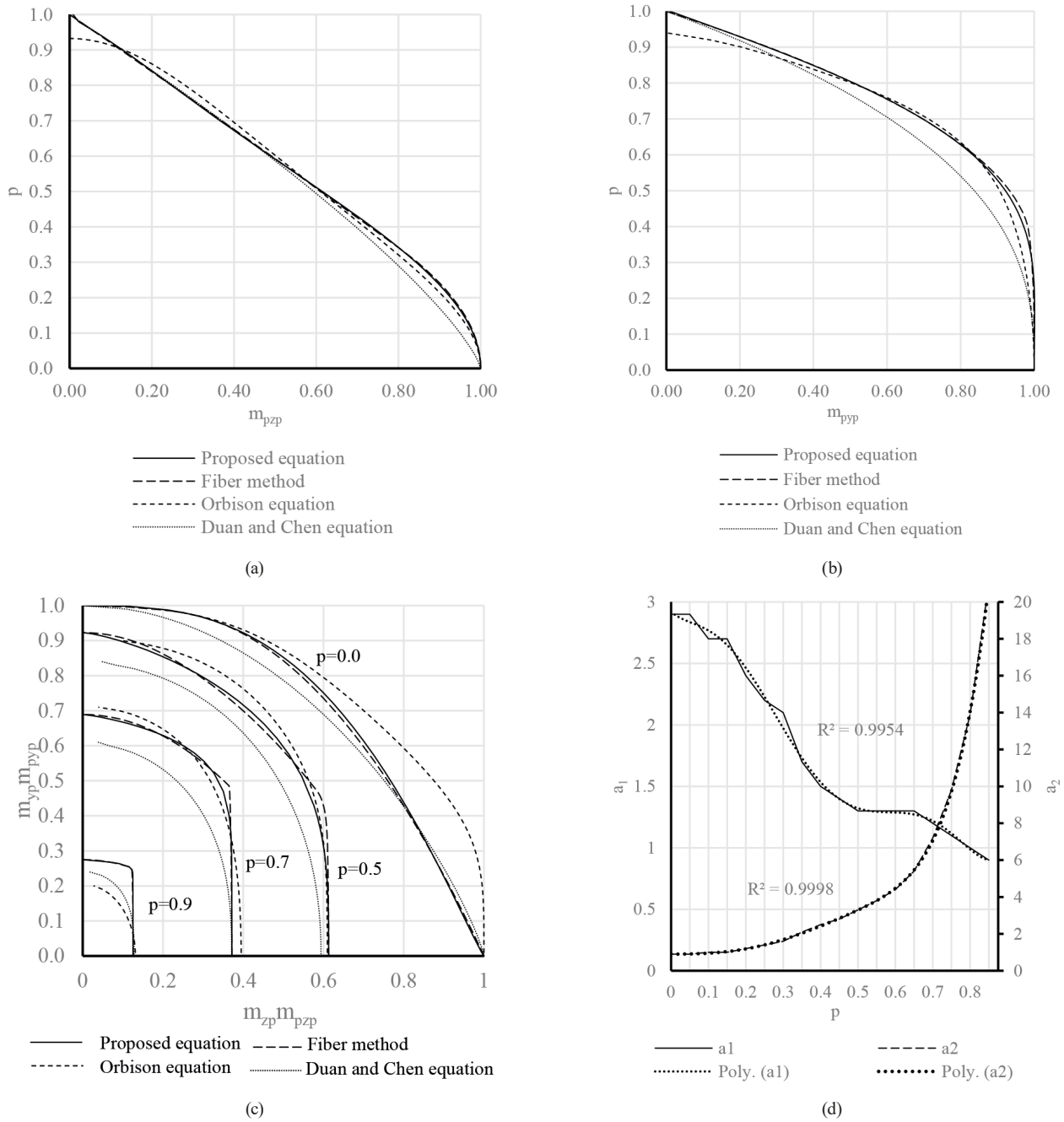

Fig. 8 Yield surfaces for W12 × 30 section: (a) p-m_{pzp}, (b) p-m_{pyp}, (c) Plane view, (d) a_1 and a_2 parameters

Table 4 Parameters for $m_{py}m_{pzp}$-$m_{pz}m_{pyp}$ interaction curves

Index	W12 × 30		HSS12 × 12 × 1/2
	d	e	d and e
1	207.80	1696.23	96.62
2	−535.07	−3649.69	−200.03
3	483.74	2992.69	149.70
4	−171.76	−1140.12	−36.85
5	15.64	205.63	1.04
6	−1.55	−11.92	0.87
7	2.90	0.90	1.70
R^2	0.9954	0.9998	0.9998

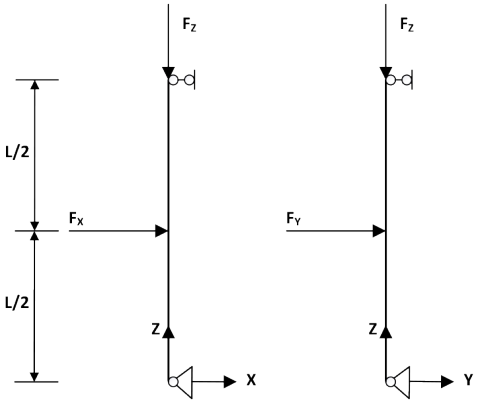

Fig. 9 Geometry and applied loads of the column

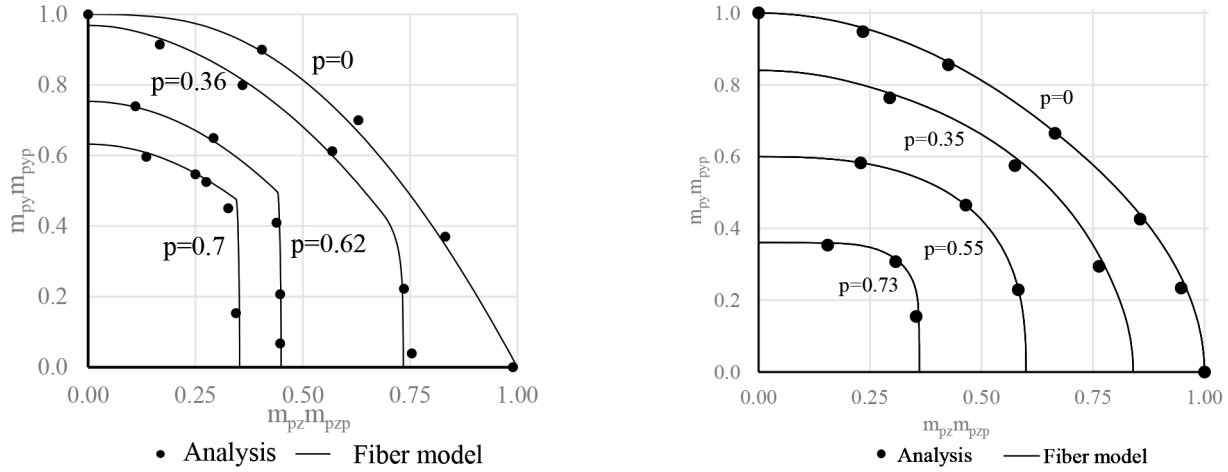

Fig. 10 Nomalized forces at midspan: (a) W6 × 20, (b) HSS6 × 6 × 1/4

Table 5 Comparison of solution time (s)

Number of elements	Fiber method	Proposed method
2	21	2
10	15	2
100	127	2
200	253	3

5.3 Space steel frame

The two-story space frame shown in Fig. 11 (a) was previously analyzed by Zubydan [12]. The yield strength, Young's modulus, and Poisson's ratio of all members are 320 MPa, 221000 MPa, and 0.3, respectively. H150 × 150 × 10 × 6.5 section is used for all elements where the strong axis of the columns is in *Y*-direction. The cross section has P_y = 1230 kN, M_{py} = 364 kN m and M_{pz} = 760 kN m and parameters for the yield surface are presented in Table 6 and Table 7. The node and element number are shown in Fig. 11 (b) for the finite element model. The vertical and lateral loads were applied proportionally until the frame reaches the failure state in two analysis cases. The plastic hinges are assumed to be formed only at the ends of each element coupled with the yield surface. Fig. 12 shows results for the first analysis case in which lateral load was applied in *X*-direction only (r = 0). The ultimate lateral capacity

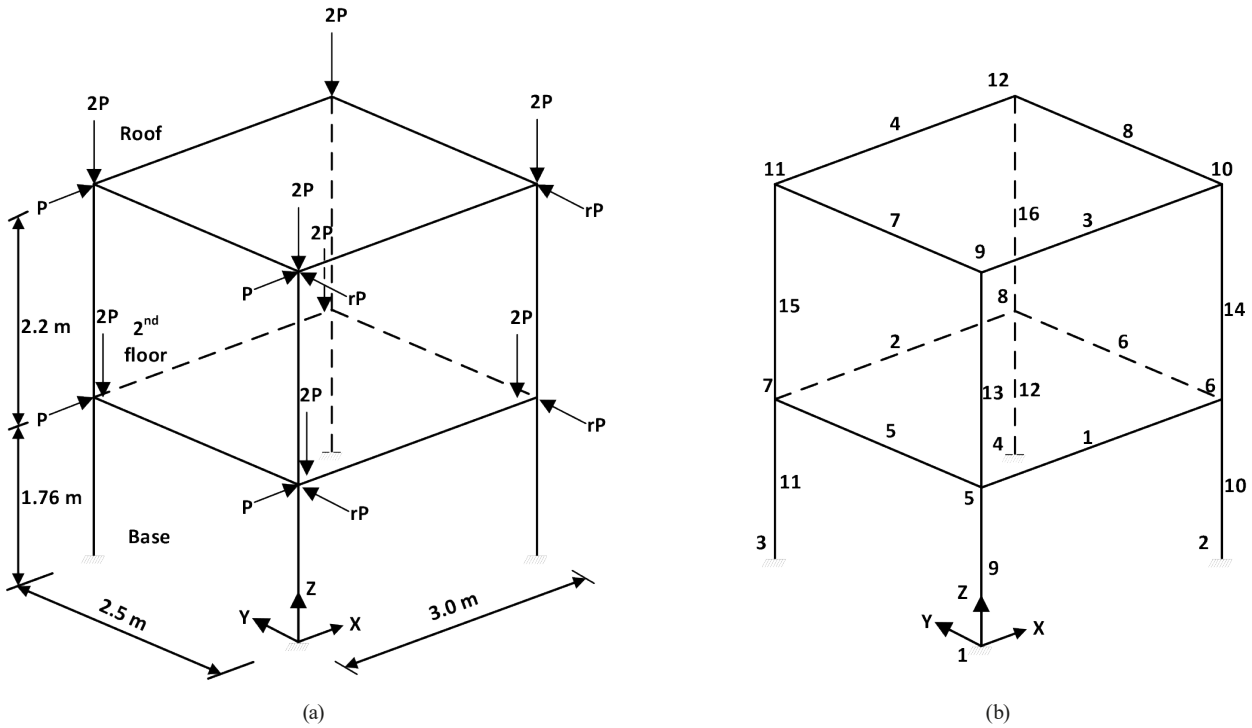

Fig. 11 Three-dimensional two-story steel frame: (a) Geometry and applied loads, (b) Node and element numbers

Table 6 Parameters for p-m_{pyp} and p-m_{pzp} of H150 × 150 × 10 × 6.5 section

Index	b	c
1	−1.01	0.63
2	2.09	−1.35
3	−2.09	−0.28

Table 7 Parameters for $m_{py}m_{pzp}$-$m_{pz}m_{pyp}$ of H150 × 150 × 10 × 6.5 section

Index	d	e
1	−20.83	−48.61
2	116.51	628.69
3	−215.95	−963.27
4	175.51	529.13
5	−60.05	−94.11
6	3.50	6.94
7	2.50	0.88

of the frame ($P \sim 75$ kN) in X-direction obtained from the proposed model, fiber model and the published analysis results are in very well agreement as shown in Fig. 12 (a). The load-displacement relationships obtained from the proposed model are slightly lower than those obtained from the fiber model and Zubydan [12] before reaching failure load. The ultimate loads obtained from the proposed method is $P_u = 75.76$ kN, compared to $P_u = 75.36$ kN from the fiber model and $P_u = 75.6$ kN from Zubydan [12].

In this frame, the failure state is controlled by the failure of four columns in the first story. Consider element 9, the bending moment M_z at the bottom (node 1) reached its maximum in the proposed model, while it continued to increase in the fiber model at $P = 60$ kN. As a result, the element is weaker in the proposed model compared to the fiber model, as the load-displacement curves from the proposed method lie below those from the fiber model before failure as shown in Fig. 12 (a).

In the second analysis case ($r = 1$), the lateral loads were applied in both directions. It is clearly observed that the results obtained from the proposed model corelate well with the results obtained from the fiber model in terms of lateral capacity and load-displacement relationships (Fig. 13 (a)). The lateral capacity of the frame is greatly reduced with the increase of lateral loads in Y-direction due to the increase of bending moments produced about the weak axis of the cross section, in comparison to that of the first case. As shown in Fig. 13 (b), the internal forces of element 9 started yielding at $P = 20$ kN at the bottom while it was still in the elastic range in the proposed model. This behavior explained why the load-displacement curves from the fiber model are lower than that from the proposed model beyond the applied load of 20 kN as shown in Fig. 13 (a).

5.4 Steel portal frame

The steel portal frame shown in Fig. 14 consists of a W12 × 27 wide flange beam and two W12 × 50 columns. This frame has been analyzed by Liew et al. [20], with plastic hinges allowed to form only at the two ends of each element. The geometry and section properties of the frame are illustrated in Fig. 14. The frame is subjected to both vertical and lateral loads applied proportionally. The yield strength of all elements is $f_y = 248.2$ MPa and Young's modulus is $E = 20$ GPa. The parameters for yield surface for cross sections of the beam and columns are given in Tables 8 and 9.

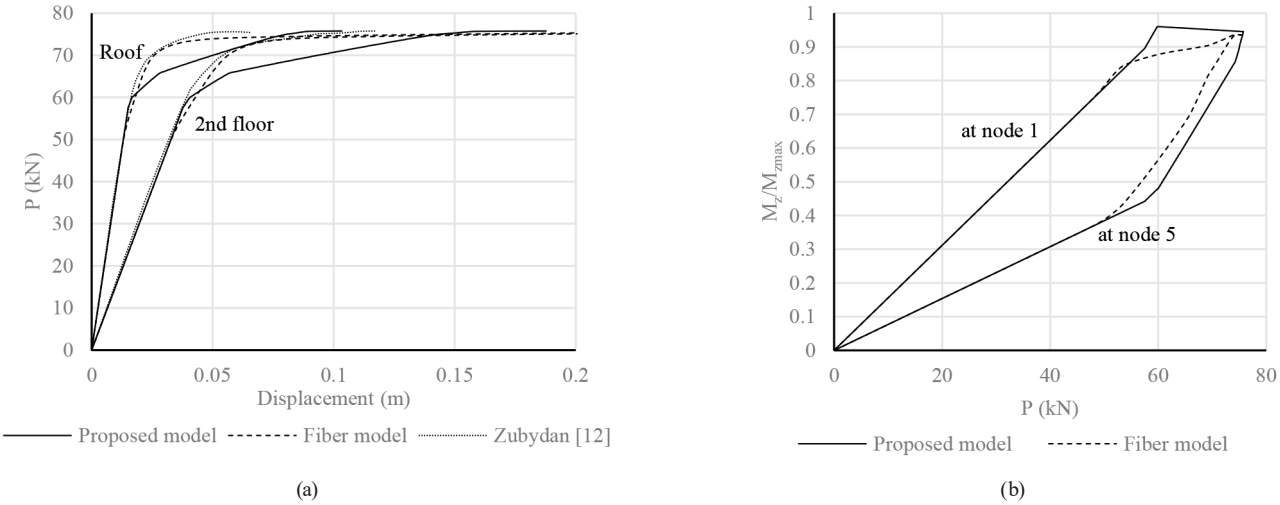

Fig. 12 Load-displacement and load-internal force relationships for the two-story frame ($r = 0$): (a) Load-displacement curve in X-direction, (b) Internal force-load curves for element 9

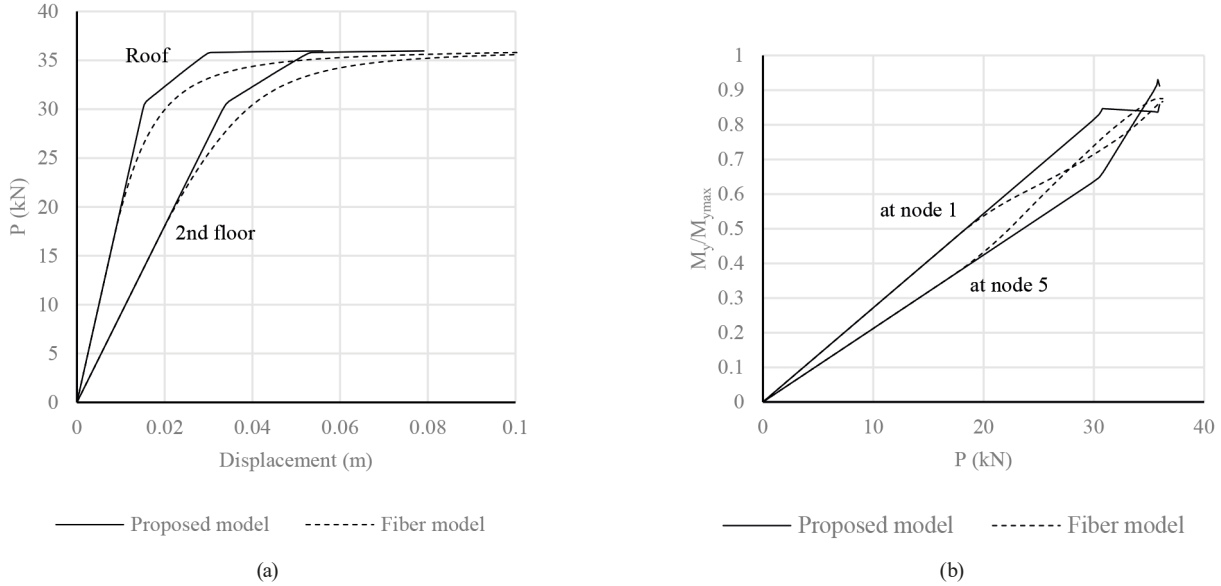

Fig. 13 Load-displacement and load-internal force relationships for the two-story frame (r = 1): (a) Load-displacement curve in Y-direction, (b) Internal force-load curves for element 9

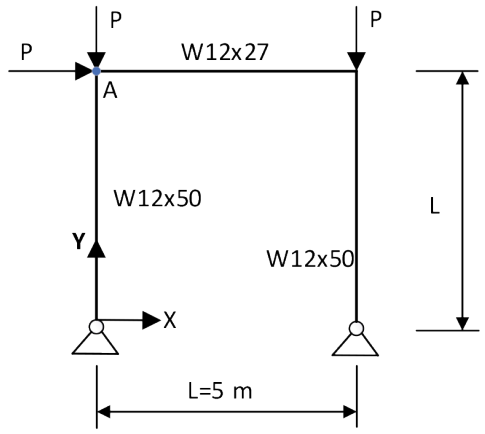

Fig. 14 Steel portal frame

Table 8 Parameters for p-m_{pyp} and p-m_{pzp}

Index	W12 × 50		W12 × 27	
	b	*c*	*b*	*c*
1	−0.84	0.71	−0.65	0.74
2	1.82	−1.61	1.54	−1.83
3	−2.00	−0.09	−1.89	0.10

Table 9 Parameters for mpympzp-mpzmpyp

Index	W12 × 50		W12 × 27	
	d	*e*	*d*	*e*
1	92.28	1821.02	219.15	1504.88
2	−236.94	−4150.66	−586.87	−3212.45
3	201.45	3581.64	563.01	2613.29
4	−52.55	−1429.12	−225.19	−991.30
5	−5.37	268.31	31.85	181.39
6	0.01	−16.92	−3.19	−11.03
7	2.58	1.05	2.83	0.98

The nonlinear behavior, represented by the load-displacement curves at point A, computed by the proposed method, is compared with that provided by Liew et al. [20] in Fig. 15 with excellent agreement. The ultimate loads obtained are 61.6 kN from the proposed method and 62.2 from Liew et al. [20].

6 Conclusions

The yield surfaces of thin-walled pipe, thin-walled box, and wide-flange sections under axial force combined with biaxial bending moments have been developed for nonlinear analysis of the steel frame. The proposed yield surfaces comprise twenty best-fitting parameters which can be determined using the power and polynomial regressions of the interaction curves. The cutting plan algorithm

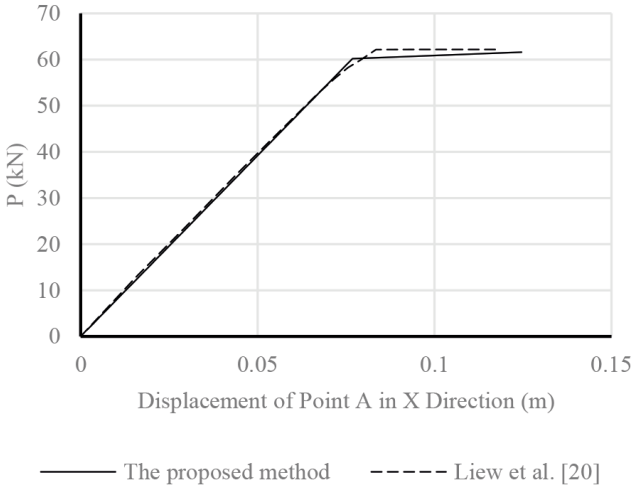

Fig. 15 Load-displacement curves for the steel portal frame

(CPA) was employed for internal force update to satisfy yield conditions in the plastic hinges. The proposed yield surfaces have been verified by comparing the predicted results using computer code SPH with those retrieved from the fiber model and the literature. The analysis results show that the proposed yield surfaces compare very well to those from the fiber model, meaning in overcoming the shortcoming the yield surfaces in the literature. In addition, the proposed model can reduce the solution time in comparison to the fiber model and capture accurately the failure load of the steel frames. Future work is envisaged considering the gradual yielding plastic hinges and spreading of plasticity along the elements using the plastic hinge concept coupled with the yield surface.

References

[1] Taucer, F., Spacone, E., Filippou, F. C. "A Fiber Beam-Column Element for Seismic Response Analysis of Reinforced Concrete Structures", [pdf] Earthquake Engineering Research Center, College of Engineering, University of California, Berkeley, CA, USA, Rep. UCB/EERC-91/17, 1991. Available at: https://nehrpsearch.nist.gov/static/files/NSF/PB94117629.pdf

[2] Ngo, H.-C., Kim, S.-E. "Practical advanced analysis of space steel frames using fiber hinge method", Thin-Walled Structures, 47(4), pp. 421–430, 2009. https://doi.org/10.1016/j.tws.2008.08.007

[3] Liu, Y.-S., Li, G.-Q. "A nonlinear analysis method of steel frames using element with internal plastic hinge", Advanced Steel Construction, 4(4), pp. 341–352, 2008. https://doi.org/10.18057/IJASC.2008.4.4.5

[4] Ngo, H.-C., Kim, S.-E. "Practical nonlinear analysis of steel–concrete composite frames using fiber–hinge method", Journal of Constructional Steel Research, 74, pp. 90–97, 2012. https://doi.org/10.1016/j.jcsr.2012.02.018

[5] Nguyen, P. C., Kim, S. E. "Second-order spread-of-plasticity approach for nonlinear time-history analysis of space semi-rigid steel frames", Finite Elements in Analysis and Design, 105, pp. 1–15, 2015. https://doi.org/10.1016/j.finel.2015.06.006

[6] Chiorean, C. G. "Computerised interaction diagrams and moment capacity contours for composite steel-concrete cross-sections", Engineering Structures, 32(11), pp. 3734–3757, 2010. https://doi.org/10.1016/j.engstruct.2010.08.019

[7] Orbison, J. G., McGuire, M., Abel, J. F. "Yield surface application in nonlinear steel frame analysis", Computer Methods in Applied Mechanics and Engineering, 33(1–3), pp. 557–573, 1982. https://doi.org/10.1016/0045-7825(82)90122-0

[8] Duan, L., Chen, W. F. "A yield surface equation for doubly symmetrical sections", Engineering Structures, 12(2), pp. 114–119, 1990. https://doi.org/10.1016/0141-0296(90)90016-L

[9] Santathadaporn, S., Chen, W. F. "Interaction curves for sections under combined biaxial bending and axial force", Fritz Engineering Laboratory, Department of Civil Engineering, Leigh University, Rep. 331.3, 1968. [online] Available at: https://preserve.lehigh.edu/lehigh-scholarship/faculty-and-staff-publications/fritz-lab-reports/interaction-curves-sections

[10] Vu, A. Q., Hoang, N. H., Nghiem, H. M. "An efficient method for yield and failure surfaces of the steel i-section", Advanced Steel Construction, 16(3), pp. 246–254, 2020. https://doi.org/10.18057/IJASC.2020.16.3.6

[11] Morris, G. A., Fenves, S. J. "Approximate yield surface equations", Journal of Engineering Mechanics Division, 95(4), pp. 937–954, 1969. https://doi.org/10.1061/JMCEA3.0001148

[12] Zubydan, A. H. "Inelastic large deflection analysis of space steel frames including H-shaped cross sectional members", Engineering Structures, 48, pp. 155–165, 2013. https://doi.org/10.1016/j.engstruct.2012.09.024

[13] Sharaf, T., Hanefa, A., Zubydan, A. H., Elghandour, M., Elsabbagh, A. "Axial Force and Biaxial Bending Interaction for I-Shaped Cross Section", Practice Periodical on Structural Design and Construction, 26(4), 04021042, 2021. https://doi.org/10.1061/(ASCE)SC.1943-5576.0000609

[14] ElSabbagh, A., Hanefa, A., Zubydan, A. H., ElGhandour, M., Sharaf, T. "Inelastic large deflection analysis of space steel frames consisting of I-shaped cross section", Steel and Composite Structures, An International Journal, 41(6), pp. 887–898, 2021. https://doi.org/10.12989/scs.2021.41.6.887

[15] Zubydan, A. H., ElSabbagh, A. I., Sharaf, T., Farag, A. E. "Inelastic large deflection analysis of space steel frames using an equivalent accumulated element", Engineering Structures, 162, pp. 121–134, 2018. https://doi.org/10.1016/j.engstruct.2018.01.059

[16] Smith, I. M., Griffiths, D. V., Margetts, L. "Programming the Finite Element Method", John Wiley & Sons, 2004. ISBN 9781119973348 https://doi.org/10.1002/9781119189237

[17] Belytschko, T., Liu, W. K., Moran, B., Elkhodary, K. "Nonlinear finite elements for continua and structures", John Wiley & Sons, 2000. ISBN 9780471987741

[18] Huang, J., Griffiths, D. V. "Return Mapping Algorithms and Stress Predictors for Failure Analysis in Geomechanics", Journal of Engineering Mechanics, 135(4), pp. 276–284, 2009. https://doi.org/10.1061/(ASCE)0733-9399(2009)135:4(276)

[19] Matias Silva, W. T., Mendes Bezerra, L. "A Radial Return Algorithm Application in Elastoplastic Frame Analysis Using Plastic Hinge Approach", Mathematical Problems in Engineering, 2010(1), 142743, 2010. https://doi.org/10.1155/2010/142743

[20] Liew, J. R., Chen, H., Shanmugam, N. E. "Inelastic Analysis of Steel Frames with Composite Beams", Journal of Structural Engineering, 127(2), pp. 194–202, 2001. https://doi.org/10.1061/(ASCE)0733-9445(2001)127:2(194)

Appendix

If plastic hinges formed at one end of the element:

1. Initialization: set initial values of plastic displacement to converged values at end of previous load step, zero the incremental plasticity parameter, and evaluate the elastic trial forces:

$$k = 0;\ \boldsymbol{u}_p^{(0)} = \boldsymbol{u}_{p,n};\ \lambda^{(k)} = 0;$$
$$\boldsymbol{F}^{(0)} = \boldsymbol{K}\left(\boldsymbol{u}_{n+1} - \boldsymbol{u}_p^{(0)}\right).$$

2. Check yield condition and convergence at k^{th} iteration $f_{(k)} < \text{TOL}$, converged else go to 3. TOL is convergence tolerance of the iteration.
3. Compute increment in plasticity parameter

$$\lambda = \frac{f^{(k)}}{\boldsymbol{q}^{(k)}\boldsymbol{K}\boldsymbol{r}^{(k)}}.$$

4. Obtain force increments

$$\Delta\boldsymbol{F}^{(k)} = -\lambda^{(k)}\boldsymbol{K}\boldsymbol{r}^{(k)}.$$

5. Update plastic strains and forces

$$\boldsymbol{u}_p^{(k+1)} = \boldsymbol{u}_p^{(k)} + \Delta\boldsymbol{u}_p^{(k)} = \boldsymbol{u}_p^{(k)} + \lambda^{(k)}\boldsymbol{r}^{(k)}$$

$$\boldsymbol{F}^{(k+1)} = \boldsymbol{F}^{(k)} + \Delta\boldsymbol{F}^{(k)}$$

$k \to k + 1$ go to 2.

If plastic hinges formed at both ends of the element:

1. Initialization: set initial values of plastic displacement to converged values at end of previous load step, zero the incremental plasticity parameter, and evaluate the elastic trial forces:

$$k = 0;\ \boldsymbol{u}_p^{(0)} = \boldsymbol{u}_{p,n};\ \lambda_1^{(0)} = 0;\ \lambda_2^{(0)} = 0;$$
$$\boldsymbol{F}^{(0)} = \boldsymbol{K}\left(\boldsymbol{u}_{n+1} - \boldsymbol{u}_p^{(0)}\right).$$

2. Check yield condition and convergence at k^{th} iteration $f_1^{(k)} < \text{TOL1}; f_2^{(k)} < \text{TOL2}$ converged else go to 3. TOL1 and TOL2 are convergence tolerances of the iteration.
3. Compute increment in plasticity parameters

$$\lambda_1^{(k)} = \frac{f_2^{(k)}\boldsymbol{q}_1^{(k)}\boldsymbol{K}\boldsymbol{r}_2^{(k)} - f_1^{(k)}\boldsymbol{q}_2^{(k)}\boldsymbol{K}\boldsymbol{r}_2^{(k)}}{\boldsymbol{q}_2^{(k)}\boldsymbol{K}\boldsymbol{r}_1^{(k)}\boldsymbol{q}_1^{(k)}\boldsymbol{K}\boldsymbol{r}_2^{(k)} - \boldsymbol{q}_1^{(k)}\boldsymbol{K}\boldsymbol{r}_1^{(k)}\boldsymbol{q}_2^{(k)}\boldsymbol{K}\boldsymbol{r}_2^{(k)}}$$
$$\lambda_2^{(k)} = \frac{f_1^{(k)}\boldsymbol{q}_2^{(k)}\boldsymbol{K}\boldsymbol{r}_1^{(k)} - f_2^{(k)}\boldsymbol{q}_1^{(k)}\boldsymbol{K}\boldsymbol{r}_1^{(k)}}{\boldsymbol{q}_2^{(k)}\boldsymbol{K}\boldsymbol{r}_1^{(k)}\boldsymbol{q}_1^{(k)}\boldsymbol{K}\boldsymbol{r}_2^{(k)} - \boldsymbol{q}_1^{(k)}\boldsymbol{K}\boldsymbol{r}_1^{(k)}\boldsymbol{q}_2^{(k)}\boldsymbol{K}\boldsymbol{r}_2^{(k)}}.$$

4. Obtain force increments

$$\Delta\boldsymbol{F}^{(k)} = -\lambda_1^{(k)}\boldsymbol{K}\boldsymbol{r}_1^{(k)} - \lambda_2^{(k)}\boldsymbol{K}\boldsymbol{r}_2^{(k)}.$$

5. Update plastic strains and forces

$$\boldsymbol{u}_p^{(k+1)} = \boldsymbol{u}_p^{(k)} + \Delta\boldsymbol{u}_p^{(k)} = \boldsymbol{u}_p^{(k)} + \lambda_1^{(k)}\boldsymbol{r}_1^{(k)} + \lambda_2^{(k)}\boldsymbol{r}_2^{(k)}$$

$$\boldsymbol{F}^{(k+1)} = \boldsymbol{F}^{(k)} + \Delta\boldsymbol{F}^{(k)}$$

$k \to k + 1$ go to 2.

In all equations above, subscripts 1 and 2 represent the first and second ends of the element, respectively.